



OPEN ACCESS

Laser heating of large noble gas clusters: from the resonant to the relativistic interaction regimes^{*}

To cite this article: E T Gumbrell *et al* 2008 *New J. Phys.* **10** 123011

View the [article online](#) for updates and enhancements.

You may also like

- [Ensemble effects on the reconstruction of attosecond pulses and photoemission time delays](#)
F Vismarra, R Borrego-Varillas, Y Wu et al.
- [Coulomb asymmetry and sub-cycle electron dynamics in multiphoton multiple ionization of H₂](#)
M Spanner, S Gräfe, S Chelkowski et al.
- [Complementary diagnostics of high-intensity femtosecond laser pulses via vacuum acceleration of protons and electrons](#)
O E Vais and V Yu Bychenkov

Laser heating of large noble gas clusters: from the resonant to the relativistic interaction regimes*

E T Gumbrell^{1,2,4}, A S Moore^{1,2}, J A Lazarus²,
E L Clark^{1,5}, P M Nilson^{2,6}, W J Garbett¹, A J Comley¹,
J S Robinson², M Hohenberger², R D Edwards¹, R E Eagleton¹,
R J Clarke³, D R Symes^{2,3} and R A Smith²

¹ Plasma Physics Division, AWE Aldermaston, Reading RG7 4PR, UK

² Blackett Laboratory, Imperial College, London SW7 2BZ, UK

³ Rutherford Appleton Laboratory, Chilton OX11 0QX, UK

E-mail: edward.gumbrell@awe.co.uk and r.a.smith@imperial.ac.uk

New Journal of Physics **10** (2008) 123011 (19pp)

Received 14 April 2008

Published 9 December 2008

Online at <http://www.njp.org/>

doi:10.1088/1367-2630/10/12/123011

Abstract. Wide-ranging measurements of sub-picosecond laser interactions with large noble gas cluster targets have been conducted in order to help clarify the nature and extent of the underlying laser–plasma heating. Within the sub-relativistic vacuum irradiance range of 10^{16} – 10^{17} W cm⁻², we find that electron temperatures measured with continuum x-ray spectroscopy exhibit a pronounced multi-keV enhancement. Analysis indicates this behaviour to be consistent with collisional or collisionless resonant heating mechanisms. We also present the first measurements of laser-to-cluster energy deposition at relativistic vacuum irradiances, our data demonstrating absorption fractions of 90% or more. Optical probing was used to resolve the onset of a supersonic ionization front resulting from this very high absorption, and shows that despite significant pre-focus heating, the greatest plasma energy densities can be generated about the vacuum focus position. Electron energy spectra measurements confirm that laser–plasma super-heating occurs, and together with ion data establish that

⁴ Author to whom any correspondence should be addressed.

⁵ Current address: Department of Electronics, Technological Educational Institute of Crete, Romanou 3, 73133 Chania, Crete, Greece.

⁶ Current address: Laboratory for Laser Energetics, University of Rochester, Rochester, NY 14623, USA.

*© British Crown Copyright 2008/MOD

relativistic laser–plasma coupling in atomic clusters can take place without significant MeV particle beam production. In conjunction with optical self-emission data, the optical probing also indicates laser pre-pulse effects at peak vacuum irradiance of $5 \times 10^{19} \text{ W cm}^{-2}$. Laser absorption, plasma heating and energy transport data are supported throughout with analytical and numerical modelling.

Contents

1. Introduction	2
2. Experimental methods	3
2.1. Lasers systems	3
2.2. Targets and diagnostics	4
3. Plasma temperature measurements from krypton clusters heated using subrelativistic laser irradiances	5
3.1. Electron temperature variation with laser irradiance	5
3.2. Collisional heating and nanoplasma modelling	6
3.3. Collisionless heating estimates	7
3.4. Summary	8
4. Calorimetric, optical, electron and ion measurements from xenon clusters subjected to relativistic vacuum irradiances	8
4.1. Laser–cluster absorption data	8
4.2. Analysis of absorption data considering single cluster and extended spatial effects	9
4.3. Sub-picosecond optical probing	10
4.4. Absorption modelling	12
4.5. Electron heating estimates	12
4.6. Electron and ion data with analysis	13
4.7. Plasma energy transport analysis and modelling	14
4.8. Laser pre-pulse effects and self-emission data	15
5. Conclusions and future directions	17
Acknowledgments	18
References	18

1. Introduction

Gas cluster targets, which are essentially ensembles of sub-optical wavelength-scale, near solid density atomic or molecular aggregates, occupy an intermediate range of sizes between those of bulk (continuous, macroscopic) solids and the unclustered atoms or molecules. In the plasmas formed from short pulse laser heating of gas clusters, the total laser energy absorption fractions (f_{abs}) attained using sub-relativistic laser irradiances ($I_0 < 10^{18} \text{ W cm}^{-2}$) can be of the order of unity, and arise from a much increased absorption coefficient $\alpha (\text{cm}^{-1})$ over unclustered gases. This, in turn, is a result of strong laser coupling to individual clusters through collisional (micro-field) [1] or collisionless (macro-field) [2] processes. Owing to the sizes and geometry involved, these coupling mechanisms differ significantly, however, from those that occur in bulk solid targets. Moreover, the fractions f_{abs} absorbed into gas clusters can exceed those from

laser irradiation of bulk solid targets [1, 3] when using the same vacuum irradiances I_0 . In this case, the fact that the absorbing clusters medium is spatially extended along the laser focus—as opposed to being delineated by a single skin-depth region—plays a key role in enhancing f_{abs} over bulk solid targets.

Globally, therefore, laser–plasma interactions with gas clusters are phenomenologically rich and varied. Nevertheless, despite a significant body of experimental data at subrelativistic laser irradiances [1], the absorption phenomena in clusters are not comprehensively understood, highlighting the need for improved experimental studies in this regime. There is also little confirmation that the anomalous laser–plasma energetics with cluster targets scales upwards with irradiance into the relativistic regime [4]. In this domain, cluster fragility ultimately limits the degree of heating that can be achieved, and the impact of both pre-pulse and pre-focus deposition needs addressing more rigorously.

This paper aims to address each of these issues with a broad series of new measurements and supporting modelling, leading to a number of significant findings. In the first instance, we detail how x-ray continuum spectroscopy has been used for the first time to directly observe resonant enhancement of the atomic cluster plasma heating in the subrelativistic regime—these data clearly demonstrate that as a result of this enhancement it is possible to create very high material energy densities (ε) in the clusters with only moderate laser energies ($E_{\text{laser}} < 1$ J) readily accessible with table-top systems. Additionally, upon scaling upwards to much higher energies and relativistic irradiances through the use of a larger facility laser [5], we find that the measured fractions f_{abs} are remarkably high, although such absorption comes with substantial pre- and post-focus energy deposition and/or the destruction of clusters from laser pre-pulse. Physically significant, moreover, is that very strong plasma heating occurs in this relativistic regime without the considerable fast particle beam generation (both electron and ion) prevalent in solid target interactions. Collectively, therefore, these data cast new light on laser–plasma interactions in atomic clusters targets, helping to advance our understanding of how these occur and, indeed, how they might be utilized.

2. Experimental methods

2.1. Lasers systems

Two Nd:glass laser systems based on chirp pulse amplification (CPA) were used in these studies: one a table-top TW laser based at Imperial College and the other a single larger facility-based system able to provide peak optical powers of many hundreds of TW, namely the Vulcan PW laser [5]. For studying nonrelativistic interactions the table-top system was used by varying the laser energy to deliver discrete values of the peak vacuum irradiance up to $I_0 = 2 \times 10^{17} \text{ W cm}^{-2}$ ($E_{\text{laser}} = 500$ mJ). In the high energy experiments the larger facility system was used to provide two discrete irradiance values of $I_0 = 5 \times 10^{18} \text{ W cm}^{-2}$ ($E_{\text{laser}} = 45$ J) and $I_0 = 5 \times 10^{19} \text{ W cm}^{-2}$ ($E_{\text{laser}} = 450$ J); here, in view of the limited shot rate, we used a $\pm 10\%$ shot-to-shot energy bin. Common to both systems was the central laser wavelength ($\lambda_0 = 1054$ nm) and full-width at half-maximum (FWHM) pulse duration ($\Delta t = 500$ fs, measured by single-shot 2nd order autocorrelation). Such commonality helps to achieve meaningful scalings from the sub-relativistic to the relativistic interaction regimes by comparison of the plasma conditions that can be attained with each laser.

Although pre-pulse effects were negligible across much of the very broad irradiance range that was accessible, they inevitably begin to change the details of the interactions at some point within the relativistic regime. In fact, for a constant pre-pulse irradiance contrast level (I_{pre}/I_0), even nominally high-contrast short pulse lasers employing a high gain-stage using Optical Parametric CPA, such as used here [5], can preionize clusters once the I_0 value is sufficiently high. When this occurs the direct scalability between the two laser systems starts to break down, although the prevailing physics is still of significant interest owing to scant empirical data covering this interaction regime. As subsequently explained, optical measurements indicated that pre-pulse effects had a significant impact for the very highest irradiance conditions used.

2.2. Targets and diagnostics

The target media were atomic clusters of Kr or Xe, produced using a solenoidal gas jet positioned in vacuum with its symmetry axis aligned perpendicular to the laser focus (coordinate values $z = 0$, $r = 0$). The same jet was used throughout these two studies (sub-relativistic and relativistic), and operating at room temperature produced a 45° half-angle plume of clusters. *In situ* Rayleigh scattering of a visible CW laser confirmed cluster formation, and from Hagen parameter scalings [6] the average cold cluster radii for Kr and Xe were $R_{c0} \approx 13$ and 23 nm, respectively.

For the subrelativistic interactions, Kr clusters were used exclusively. This is because the free–free and free–bound transition energies between the K- and L-shell emission lines of Kr are well suited to detection with a back-thinned CCD, making it particularly amenable to continuum temperature measurements based on x-ray photon counting. Using a calibrated 16-bit Andor DX434 CCD camera in vacuum, with a 25 micron Be filter, single-shot spectra were recorded for energies up to 10 keV as the laser irradiance was varied. The detector was cooled to reduce noise for accurate photon counting. The filter response, detector quantum efficiency and event-splitting were all deconvolved post-shot.

Optical, electron or ion measurements were not taken in the sub-relativistic regime because a significant body of such data already exists. However, the same is not true for the relativistic case, and in this paper, we provide data for this regime for the first time. One key issue, however, with relativistic irradiances is that the laser electric field can freely and rapidly strip plasma electrons from even very large clusters, making it challenging to efficiently couple-in the laser energy. For this reason, and because of concerns over pre-pulse effects with the higher energy laser, Xe was chosen over Kr for the relativistic studies to make larger, greater individually charged clusters, on account of the higher atomic number ($Z = 54$ against $Z = 36$), to counter rapid disassembly.

Measurements of the laser energy transmitted through the Xe clusters were made with a large area pyroelectric calorimeter placed behind the jet, shown in figure 1. Transport of energy from the interaction region was observed through optical probing, a small part of the heating beam being split off and frequency-doubled to provide a sub-ps probe for interferometric or shadowgraphic images; the 90° side-scattered 1054 nm light was also imaged. Electron energy spectra were obtained with an on-axis magnetic spectrometer and high-resolution image plate detector (Fuji BAS1800II) corrected for nonlinearities in the response to lower energy electrons. Additionally, a Thompson parabola located at $\approx 90^\circ$ to target normal, just above the injection of the probe, was set to measure fast ions.

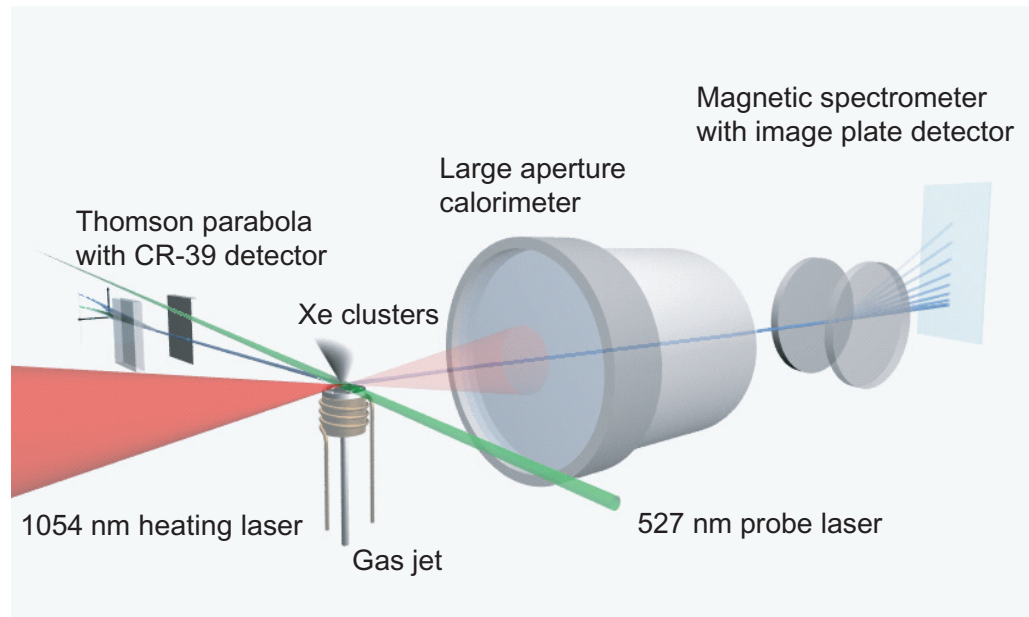


Figure 1. Schematic diagram of the diagnostics setup for experiments to characterize high-energy, sub-ps laser heating of a clustered Xe gas target. The calorimeter and the magnetic spectrometer could not be used together on the same shots as placement of the calorimeter in the laser beam transmitted through the clustered gas prevented electrons from reaching the spectrometer.

3. Plasma temperature measurements from krypton clusters heated using subrelativistic laser irradiances

3.1. Electron temperature variation with laser irradiance

The data in figure 2(a) show how the plasma electron temperature (T_e) scales with irradiances I_0 when the Kr clusters were irradiated with the table-top 500 fs laser system at I_0 values up to $2 \times 10^{17} \text{ W cm}^{-2}$. The $T_e(I_0)$ scalings are determined from exponential fits (spectral intensity $I_\nu \sim e^{-h\nu/k_B T_e}$) to the post-processed continuum spectra, examples of which are shown in the inset of figure 2(b). The T_e values are remarkably high in view of the sub-Joule laser energy employed, the multi-keV temperatures being typically greater than those in macroscopic solid targets heated by short pulses at these irradiances. The data demonstrate an approximately linear increase ($T_e \sim I_0$) from $I_0 = 4 \times 10^{16} \text{ W cm}^{-2}$ towards a strong thermal peak of $T_e^{\text{max}} \approx (4.2 \pm 0.4) \text{ keV}$ at a value $I_0^{\text{opt}} = 6 \times 10^{16} \text{ W cm}^{-2}$ —this contrasts with [7], where, for a shorter pulse duration of $\Delta t = 60 \text{ fs}$, a similar enhancement was not observed with Kr clusters. Accounting for the contribution made by the specific heat (namely energy going into excitation, ionization and heating of free electrons), our data show that both the unit length absorption α and the fractional absorption per cluster increased towards the peak of the $T_e(I_0)$ curve. The temperature T_e^{max} corresponds to the laser quiver energy (U_p) at I_0^{opt} . Beyond I_0^{opt} the measured T_e then falls off as quickly as it rose to the peak. Overall, this behaviour seems characteristic of a resonant process.

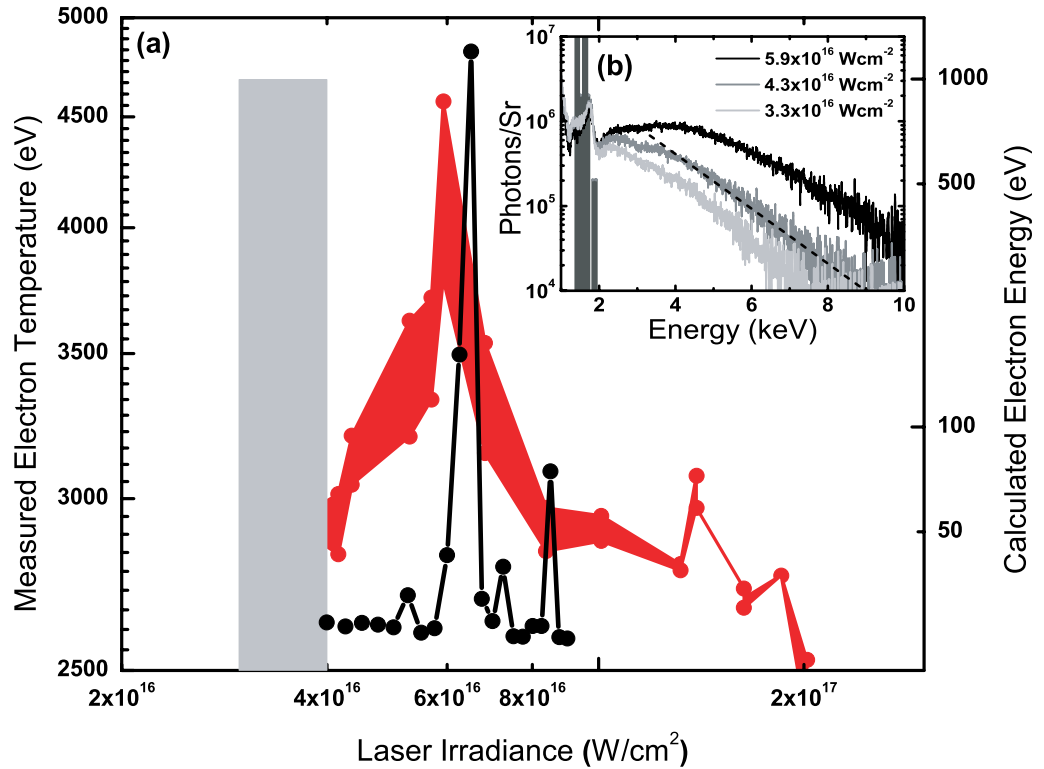


Figure 2. (a) Continuum spectroscopy measurements of free electron temperatures T_e in Kr clusters determined as a function of peak vacuum irradiance I_0 (red curve). Overlaid are the results of hydrodynamic nanoplasma simulations of collisional heating (black curve). For comparison, the grey shaded region indicates the estimated threshold irradiance values I_{th} for resonant collisionless heating. The inset, (b), shows sample deconvolved spectral data from which the points defining $T_e(I_0)$ are determined. Errors in these measured temperatures derive principally from the uncertainties in line fitting to the continuum slopes, and are indicated in the data shown in (a). As would be expected for a hot Kr plasma, line emission is evident just below 2 keV.

3.2. Collisional heating and nanoplasma modelling

In order to help explain the observed scaling of T_e with I_0 , we use a widely tested hydrodynamic nanoplasma model [8]. While comparatively simple (it assumes, for example, uniform density profiles in expanding cluster plasmas), this model captures key aspects of the underlying physics and describes, quite crucially, how ultrafast electrostatic (sub-wavelength scale) modification of the laser \mathbf{E} -field in the clusters impacts the heating. First, in order to validate the nanoplasma model in this regime, we have tested for agreement with the solution of the Maxwell equations for a small, homogeneous conductor: taking the standard Mie solution, and using a representative density $n_e/n_{crit} \approx 80$, we computationally evaluate the internal and scattered fields by summing over the partial waves to a limiting value ensuring adequate convergence. The result demonstrates that the electrostatic limit is recovered in the electromagnetic solution, corroborating the nanoplasma model insofar as quasi-neutrality is maintained, and also reveals that the skin-effect is altogether absent, as should be expected for an object of this size scale.

Nanoplasma model results are overlaid with the data in figure 2(a). While sensitive to the choice of laser pulse duration Δt and initial cluster radius R_{c0} , model results agree well with the irradiance condition I_0^{opt} and indicate an enhancement of ≈ 1 keV. We find that I_0^{opt} corresponds to the condition $n_e = 3n_{\text{crit}}$ occurring around the peak of the laser pulse ($t = t_0$), such that once $I_0 > I_0^{\text{opt}}$ the plasma expansion curtails the enhancement in the heating. That the expansion rate has a only weak scaling with temperature—it is characterized by the sound speed $c_s \sim \sqrt{Z_{\text{eff}} T_e}$, where Z_{eff} is the average ionization—underlines the inherent sensitivity in the model to the interaction parameters. In reality, this sensitivity is lessened in the experiments as the clusters explode non-uniformly with a radial density profile. This radial profile also likely prolongs the resonance [9], which may account for differences in T_e seen between model and experiment. Further, the distribution of cluster sizes inherent in the use of a gas jet source helps to explain why the (narrower) width of the simulated resonance differs from the data.

3.3. Collisionless heating estimates

The nanoplasma model, though valuable, does not adequately describe the non-quasi-neutral aspects of the interaction physics. To address these, we make combined use of the electrostatic models described in [2, 10], and extend the equations in [10] to the case where the atomic number $Z > 1$. This analytical approach also enables estimation of the temperature increase associated with collisionless heating. To commence our calculations of collisionless heating, we note that most plasma electrons would remain bound to a charged parent cluster during the laser interaction. These electrons form an ‘inner’ core with an oscillation amplitude $d_0 = 3|e|E/m_e\omega_p^2$ (E is the instantaneous electric field strength, e the electron charge, m_e the electron rest mass and ω_p the electron plasma frequency), which is small compared with the instantaneous radius of the ion background R_c [10]. When the core is strongly overdense, inverse bremsstrahlung (IB) collisional heating is precluded. For a given ion number density (n_i), there are also $N_{\text{ext}} = 4\pi Z_{\text{eff}} n_i [R_c^3 - (R_c^3 - d_0^3)]/3$ ‘outer’ electrons extracted by the laser which oscillate about the core with an amplitude of the order of the quiver motion x_{osc} —this is the so-called ‘outer ionization’. If $\omega_p \gg \omega_0$ (the laser frequency), the laser is shielded out during electron return to the parent plasma core so that these outer electrons are able to undergo collisionless heating through interplay of the laser and whole cluster electric fields. Consequently, when the electron round-trip transit time across the core corresponds to a whole cycle of the optical field, namely $2R_c\omega_0 \approx \pi v$, where v is the electron velocity, the absorption is then resonant [2]. Using these criteria, a threshold irradiance, normalized to the cluster radius, has been identified for the onset of strong collisionless absorption [2].

To help determine the threshold irradiance at the time when the quiver velocity maximizes, we begin by taking values of $Z_{\text{eff}} = 20$ and $T_e = 1.5$ keV in order to calculate that the core size from hydrodynamic expansion increases from $R_{c0} = 13$ nm to $R_c \approx R_{c0} + (c_s \Delta t/2) \approx 60$ nm. After accounting for the different λ_0 values used in [2], the corresponding threshold resonance value is then $I_{\text{th}} = 3\text{--}4 \times 10^{16}$ W cm $^{-2}$, as shown in figure 2(a). Given that the inherent systematic uncertainty in irradiance is as large as $\Delta I_0 \approx \pm 0.5 I_0$, I_{th} still falls within the measurable bounds of I_0^{opt} . Considering, moreover, that the T_e value used to estimate I_{th} is less than the lowest measured value in figure 2, the expanded core size may actually be greater, which can have the effect of bringing the calculated value for I_{th} closer to I_0^{opt} . Ultimately, as the irradiance is increased beyond I_{th} , the electron transit period changes as the quiver velocity

and cluster size evolve, resulting in dephasing of electron motion with respect to the laser field, and decreasing energy transfer to electrons via this mechanism.

Calculation of the heating effect of collisionless heating requires determination of the extracted (or outer ionized) electron fraction (Γ). For the collisionless resonance to impact T_e the fraction Γ cannot be small compared with unity; conversely, to maintain the overdense core needed for the resonance requires that $\Gamma < 1$. From the preceding expressions for d_0 and N_{ext} we estimate representative values of $d_0 \approx R_c/6$ and $\Gamma \approx 0.4$ during the main laser absorption phase. From these values, we then determine that the post-equilibration, net free electron temperature increase per laser cycle would be $\Delta T_e \approx \Gamma N_{\text{ext}} U_p / 2\pi(1 - \Gamma) k_B R_c^3 Z_{\text{eff}} n_l \approx 900$ eV. While not a detailed time-dependent calculation, comparison of this estimate with the data in figure 2(a) allows us to determine that the collisionless resonance must only be effective for a few optical cycles if it is to have caused the strong enhancement in T_e that was observed.

3.4. Summary

The experimental data we have shown provide evidence for resonant heating, and our analysis shows this to be consistent with either a collisional or a collisionless mechanism. These mechanisms are not mutually exclusive—they depend on different plasma conditions, with the nominal cross-over being $n_e \approx 10 n_{\text{crit}}$ —but the ponderomotively driven, collisionless component should generally occur earlier in the pulse when the cluster cores are more strongly overdense. Nevertheless, for a particular cluster size, the enhancements calculated from the nanoplasma and collisionless models should not occur together if they are both assumed to occur around the peak of the pulse, as was the case here.

The measurements of T_e using the continuum are spatiotemporally integrated, yet to a good approximation they refer to conditions inside the cluster plasmas at the time of peak local energy density ε . If, therefore, nanoplasma-type resonance is the principal heating mechanism, the experiment indicates a value in the locally high-density aggregates of $\varepsilon \approx 10^7$ J cm⁻³ at I_0^{opt} ($E_{\text{laser}} = 250$ mJ)—this estimate ignores additional contributions from the ion kinetic, and electron excitation and ionization energies. Such values of ε are highly transient, making the plasma conditions challenging to study, but underscore the uniqueness of gas clusters as a source of energetic particles, or as a driver of rapid energy transport processes in bulk material which are strongly decoupled from the initial laser absorption [11].

4. Calorimetric, optical, electron and ion measurements from xenon clusters subjected to relativistic vacuum irradiances

4.1. Laser–cluster absorption data

In order to address the issues surrounding laser–cluster heating at relativistic vacuum irradiances, we studied absorption by large Xe clusters of a 500 fs laser pulse with energies up to 450 J. Here, the uncertainties concern both cluster survivability at relativistic irradiances, and the type of absorption mechanisms that prevail—it is already clear from the data in section 3 that resonant heating should not generally be anticipated at relativistic irradiances.

The calorimetry measurements described in section 2 indicated 10% or lower laser energy transmission through the target on these very high energy shots. Also, optical diagnostics showed no significant side- and back-scatter, an observation that is consistent with a large initial

cluster size R_{c0} providing a cross section for absorption much greater than for scattering [12], such that any scattered and defocused light is subsequently absorbed. This shows that ionized Xe clusters are collectively near-opaque at these relativistic irradiances and high input energies, meaning that the pulse encounters so much absorbing material that it cannot ‘burn-through’ the gas jet. Specifically, we find that the target medium provides effectively unity f_{abs} , the highest efficiency $f_{\text{abs}} = 0.98$ being repeatedly attainable for 45 J pulses. The 450 J shots provided evidence for some irradiance-induced burn-through, with the measured absorption being $f_{\text{abs}} = 0.90$. In each case, the errors in f_{abs} are calculated to be insignificant.

These data, which we found to be highly repeatable, confirm greater absorption than has been measured in short pulse interactions with bulk solid targets [3]. Yet such a high absorption is not readily predictable. For example, in [13], Xe clusters of size $R_{c0} \approx 10$ nm were irradiated with a $\lambda_0 = 527$ nm and $\Delta t = 2$ ps pulse, and the observed fall-off in f_{abs} above 10^{17} W cm $^{-2}$ was attributed to cluster expansion before peak irradiance. While considering the shorter pulse that we have used ($\Delta t = 500$ fs) naturally allows for a more complete interaction before cluster plasma disassembly (on timescales of the order of a few hundred fs), the data in [13] clearly point to decreasing absorbing efficiency towards the relativistic regime. Arguably an even better comparison is the temperature data, already described in section 3 for Kr: these results, which were taken with the same key parameters λ_0 and Δt as the Xe data, indicate declining interaction efficiencies beyond $I_0 = 6 \times 10^{16}$ W cm $^{-2}$.

4.2. Analysis of absorption data considering single cluster and extended spatial effects

Observational comparisons aside, high absorption at relativistic irradiances is not to be anticipated *a priori* because the laser electric fields are able to irreversibly strip the clusters of most electrons on a very short timescale. To help understand why this is so, we begin with reference to the effects described in [14, 15], namely that the average atomic ionization Z_{eff} in a single cluster becomes enhanced as electrons get stripped off the clusters. This stripping process (outer ionization) will continue until the magnitude of the electron to cluster binding energy, which we give as $|U_c| \approx 4\pi e^2 R_c^2 n_i Z_{\text{eff}} \Gamma / 3$, is no longer exceeded by U_p , at which point the fraction Γ stabilizes. Competing against cluster charge-up from electron removal, the ion density falls off with expansion as $n_i \sim 1/R_c^3$, so if the pulse is then long enough the inner electron oscillation amplitude $d_0 \rightarrow R_c$ [10]. This has the effect of destroying the bound core required for efficient absorption.

For a peak value irradiance of $I = 5 \times 10^{18}$ W cm $^{-2}$ (the lower of the two values used in studying relativistic interactions), the preceding scalings allow us to calculate that merely a doubling of the radius under hydrodynamic expansion can be sustained by the core before dissociation, and then only if $Z_{\text{eff}} \approx Z$. In fact, for a peak value of $I = 5 \times 10^{18}$ W cm $^{-2}$, the laser pulse’s leading edge can produce T_e of a few keV, and the resulting expansion causes core dissociation prior to the interval of peak irradiance, namely $\{t_0 - (\Delta t/2) \leq t \leq t_0 + (\Delta t/2)\}$, with time $t = t_0$ being at the peak of the pulse. This dissociation significantly reduces any plasma heating. In order then to properly address the issue of cluster survivability, a limiting irradiance for efficient single cluster absorption, I_{max} , should be determined through comparison of $|U_c|$ and U_p . For the Xe cluster experiments, we calculate that $I_{\text{max}} = 10^{18}$ W cm $^{-2}$, which is an estimate valid up to an expanded radius $R_c = 5R_{c0}$.

Having considered the effect of relativistic irradiance on large single cluster absorption, we now examine the effects of the extended target medium. Here the details of the distribution

of absorbed laser energy—both spatially and to particle type and number—are of particular interest. First, and most trivially, the summation of the individual laser-cluster absorptions over the ensemble of clusters within the focus accounts for the total energy deposition. However, spatial variations in this summation are very significant due to the nonlinearities in the single cluster absorption and differences in the number of absorbers through and across the gas jet with the beam focusing. In order to determine the summation interval, namely the intra-cluster spacing, we take a cold material density $\rho = 3.6 \text{ g cm}^{-3}$ locally in each cluster and a lower bound on the spatially averaged atomic density of $3 \times 10^{18} \text{ cm}^{-3}$. Then the initial fractional volumetric fill with clusters $\beta \leq 10^{-3}$ and the intra-cluster spacing $\approx \beta^{-1/3} R_{c0} \geq 10 R_{c0} \approx 230 \text{ nm}$. Despite the low fractional volumetric fill, the spacing ensures that the laser encounters ample energy absorbing material as it propagates through the focus. For example, we can heuristically estimate the areal fill fraction of the heating beam with clusters over one Rayleigh range ($l_{\text{Rayleigh}} = 45 \mu\text{m}$) to begin at ≥ 0.2 , and then increase with plasma expansion during the interval $\{t_0 - (\Delta t/2) \leq t \leq t_0 + (\Delta t/2)\}$. Moreover, since the $R_c \ll \lambda_0$, the clusters cast no geometrical shadow, so the laser energy not absorbed by one cluster then continues to further absorbers. Consequently, as the beam focuses there is effectively complete (and repeated) sampling of the wavefronts by the clusters, which ionize on the leading edge of the pulse. Nevertheless, the laser absorption can only be as high as we have measured if the single cluster energy absorption is itself very efficient compared with the unclustered case for the same mass of material.

Even with the enhanced absorption into clusters, it is also the case that only a small fraction of laser energy can actually deposit around the best focus under the conditions studied. To see why, we suppose the opposite, namely that most absorption occurs around the position of the vacuum focus ($z = 0$), over a length $1/\alpha = 2l_{\text{Rayleigh}}$ and in a volume $\xi = \pi w^2/\alpha$ ($w \approx 15 \mu\text{m}$ is the $1/e^2$ irradiance radius). Then assuming that the bulk of the 45 J laser energy is absorbed by electrons in already highly stripped Xe cluster plasma ions (atomic ionization being energetically small compared with outer ionization), conservation of energy gives $T_e \approx E_{\text{laser}} A / e N_A Z \rho \xi \beta$, where A and Z are the mass and atomic numbers and N_A is Avogadro's constant. This estimate provides multi-MeV values for T_e , which are far too high for self-consistency because the bulk of electrons would simply free-stream away from the parent clusters at lower energies, and without the bound electron cores the high absorption could not be achieved in the first place.

4.3. Sub-picosecond optical probing

Short pulse interferometry was used as described in section 2 to interpret the absorption data by reference to spatial information on the heating and plasma expansion. The deconvolved data for $I_0 = 5 \times 10^{18} \text{ W cm}^{-2}$ ($E_{\text{laser}} = 45 \text{ J}$) in figures 3(a)–(c) show snapshots of the electron density profile $n_e(r, z)$ —deconvolution is implemented using both Abel and cylindrically symmetric Radon inversion, these two techniques showing excellent agreement. The greatest heating effect, and therefore highest ε , is seen to occur around the nominal best focus (propagation distance $z = 0$), as this is where the fastest ionization front is launched radially outward. The trajectory of this supersonic front is shown in figure 3(d). Averaged over the first 15 ps the front's speed $\bar{v}_r = \delta r_{\text{IF}} / \delta t = (1.5 \pm_{0.2}^{0.3}) \times 10^9 \text{ cm s}^{-1}$, and a power-law fit to the trajectory, $r_{\text{IF}} \sim (t - t_0)^{0.54 \pm 0.03}$, shown in figure 3(d), suggests that v_r is significantly higher close to t_0 . This is discussed further in section 4.7.

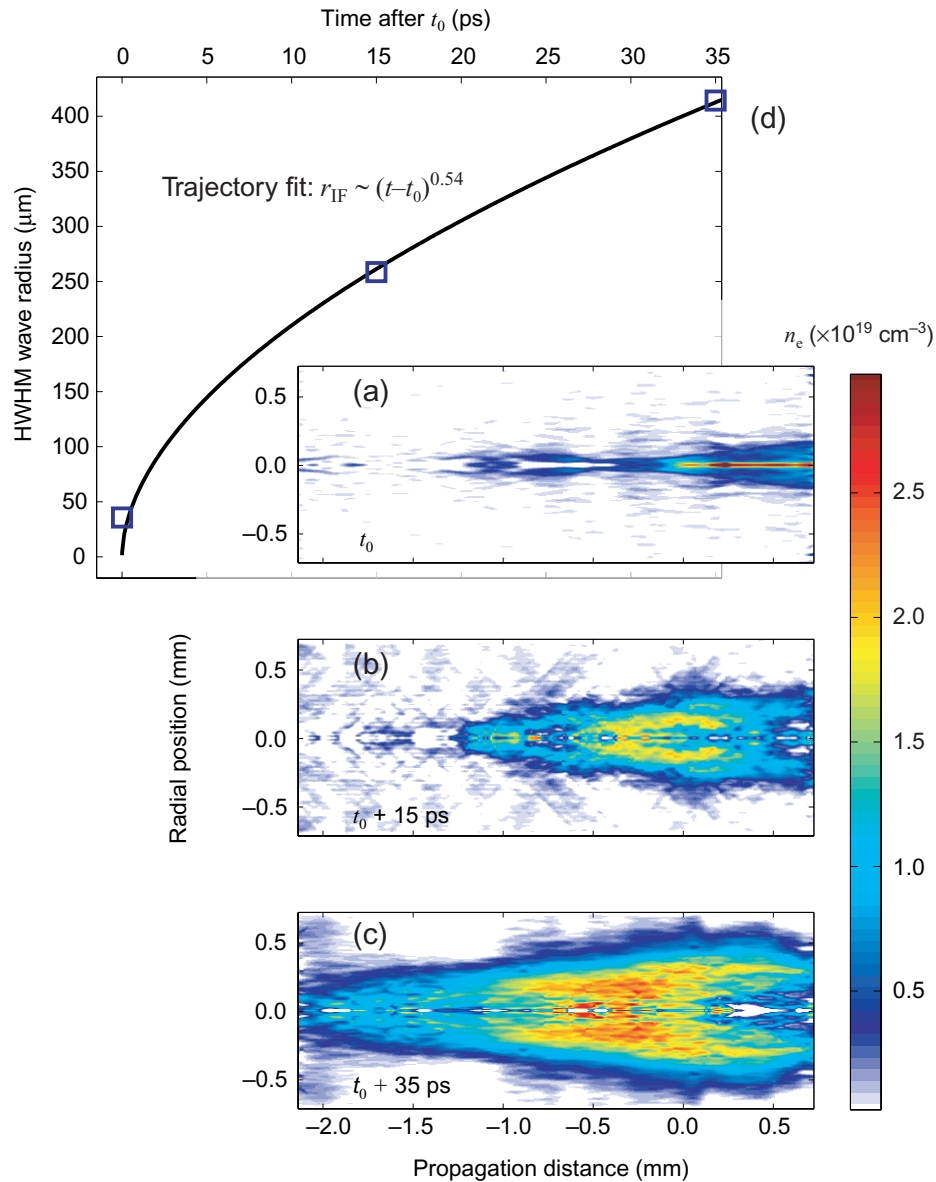


Figure 3. (a)–(c) Deconvolved electron density profiles, $n_e(r, z)$, resulting from 98% absorption of the 45 J laser pulse ($I_0 = 5 \times 10^{18} \text{ W cm}^{-2}$) into Xe clusters. The laser pulse travels from left to right, the vacuum focus location being at $z = 0$. (d) Data points (blue squares) corresponding to the HWHM values of Gaussian fits to $n_e(r, z = 0)$, and the ionization front trajectory, $r_{\text{IF}}(t, z = 0)$, calculated from a power-law fit to these data (black line). The errors in these measurements are determined from the finite pulse duration and the imaging system spatial resolution.

Figure 3(a) also indicates that the directly laser heated volume $\gg \xi$, yet this volume is itself small compared with the region subsequently heated by the ionization front, as can be seen in the later-time data of figures 3(b) and (c). Figures 3(b) and (c) also point to a significant fraction of the laser energy initially depositing before the best vacuum focus, since here the degree of relative ionization is high and the heated volume greatest.

4.4. Absorption modelling

We use the nanoplasma model as a basis for performing an integrated energetics calculation to estimate pre-focus absorption. Besides including consideration of the nonlinear single cluster absorption, this modelling also includes the wide variations in w and I through the gas jet. Firstly, the energy absorbed per cluster is calculated as a function of I ; then from the calculation of the number of clusters that experience a given irradiance I across slices of the focal region, the pulse energy is depleted accordingly. Both the density profile of the jet and variations in the focusing beam size are included in these calculations, which we benchmarked against the paper [13]. This modelling predicts effectively complete absorption hundreds of microns before best focus ($z = 0$) owing to the strong absorption properties at sub-relativistic irradiances. That these simulations do not predict a strong heating effect about $z = 0$ can be attributed to additional processes that are not explicitly considered, such as self-focusing. Nevertheless, these studies highlight the importance of pre-focus absorption in the relativistic regime, and thus in distinguishing I_0 from the peak irradiance limited by attenuation.

It is also worth noting that the collisionless resonance described for Kr clusters in section 3 should occur in the hydrodynamically expanded Xe clusters for irradiances $I \approx 1\text{--}2 \times 10^{17} \text{ W cm}^{-2}$, thereby producing multi-keV electrons and significant pre-focus deposition of its own. This further complicates the global picture of how the high energy laser pulse attenuates through the cluster jet prior to $z = 0$.

4.5. Electron heating estimates

Absorption and transport data have shown that the high energy ($E_{\text{laser}} = 45 \text{ J}$), sub-ps laser absorption in Xe clusters is extended over a volume that is large compared with the high vacuum irradiance focal cone, and that pre-focus absorption is pronounced. We have also demonstrated that despite there being an upper irradiance limit for efficient single cluster absorption ($I_{\text{max}} = 10^{18} \text{ W cm}^{-2}$) that is small compared with the peak vacuum irradiance ($I_0 = 5 \times 10^{18} \text{ W cm}^{-2}$), the heating effect of the laser is observed to be the greatest around the position of the vacuum focus ($z = 0$).

Using the estimated value of I_{max} , we are now able to calculate the IB heating around the best focus by considering that within the time-dependent electrostatic model the laser can absorb efficiently to $n_e = 6n_{\text{crit}}$ —and indeed, to somewhat higher density values. This electron density is also consistent with the clusters surviving stripping during the interval $\{t_0 - (\Delta t/2) \leq t \leq t_0 + (\Delta t/2)\}$. To calculate the IB heating we take a standard form for the nonrelativistic, high-field electron–ion collision frequency ν_{ei} from [16]; we then assume 80% pre-focus absorption (to ensure consistency with the actual peak irradiance equalling I_{max}) and a high fractional ionization of about $z = 0$. We also discount nanoplasma resonance in accordance with [15, 17, 18] (that resonance would have the effect of driving the heating irradiance strongly into the relativistic regime). Taking these parameters, we then put the temperature $T_e^{\text{IB}} \approx 2(1 - \Gamma)\nu_{ei}U_p\Delta t/3k_B$ to give an estimated value of $T_e^{\text{IB}} \approx 45 \text{ keV}$. From this calculation, which is based on only 20% (9 J) of the laser energy (45 J) reaching the best vacuum focus, the corresponding absorption length ($1/\alpha$) determined simply from energy balance shows that the near-focus IB is quite unable to use up this remaining energy, even if the heating occurs predominately at densities $< n_{\text{crit}}$. In the absence of another viable heating mechanism, this calculation, which gives an unsurprising result, means that most additional deposition occurs

post-focus. That the latter time ($t - t_0 \gg \Delta t$) results in figures 3(b) and (c) suggests that significant deposition well beyond $z = 0$ is therefore consistent with this conclusion.

Despite significant pre- and post-focus absorption, the energy absorbed per cluster is found to be greatest at about $z = 0$, and the achievable temperatures are calculated to be very substantial, although by the nature of being incoherent, the normal IB heating cannot produce T_e values that reach the quiver energy U_p corresponding to I_{\max} and λ_0 . Nevertheless, the authors of [19] propose a collective collisional mechanism specific to clusters that supposes spatial coherence in the way that each electron collides with multiple ions, meaning that v_{ei} can increase over the incoherent IB case by a factor of up to the order of the number of ions in a cluster, thereby allowing heating to the maximum kinetic energy of the electron quiver, namely $2U_p$. Based on the calculated value of $I_{\max} = 10^{18} \text{ W cm}^{-2}$, the peak attainable temperatures that can be attained in this way are then predicted to be of the order of $2U_p \approx 200 \text{ keV}$.

4.6. Electron and ion data with analysis

The electron spectrometer allowed measurements of energies $E_e > 100 \text{ keV}$ in the $+z$ -direction (along the heating laser direction). A typical electron energy spectrum is shown on a log-linear plot in figure 4. This spectrum, which is distinctively two-valued, was found to be highly repeatable. For the lower energy component a Maxwellian fit gives an electron temperature $T_{e1} = (40 \pm 12) \text{ keV}$, the error being due to line-fitting uncertainties. This measurement is consistent with our calculations for incoherent IB heating, $T_e^{\text{IB}} \approx 45 \text{ keV}$, indicating that the laser generates energy densities $\varepsilon \approx 10^8 \text{ J cm}^{-3}$ in the cluster-plasmas, a value that compares well with the bulk heating effects of short pulses on solids at the same irradiances.

Towards higher energies, a hump is in evidence at 500 keV . While we believe this may be associated with self-focusing of the laser, as subsequently described in section 4.8, its origin may ultimately reside in a complex mix of single cluster and whole beam or collective effects. Ignoring energies above 1.4 MeV , a Maxwellian fit to this higher energy component in the spectrum gives a temperature value $T_{e2} = (170 \pm_{25}^{55}) \text{ keV}$, so the estimate for coherent IB heating falls within these measurement bounds.

Despite the agreement between measured values and our simple calculations, it is clear that most laser energy is deposited away from the best focus, and also that the effects of spatial-averaging over the extended interaction region must influence the measurements. This highlights a future requirement for spatially resolved temperature measurements of the form $T_e(r, z)$.

Laser-driven gas clusters are also known as an efficient source of energetic ions [20]. This energy originates either hydrodynamically from acceleration in the sheath field of the electrons expanding ahead of the ions, or as kinetic energy in a Coulomb explosion when electrons are removed before electron pressure gradients have time to act on the ions. Here, the Thomson parabola used to measure fast ions employed a CR-39 plastic track detector that for Xe was insensitive to ion energies $E_{\text{ion}} < 13 \text{ MeV}$. No ions were measured above this threshold with either 45 J or 450 J shots.

The maximum ion energies for the case when Coulomb explosions dominate can simply be determined as $E_{\text{ion}}^{\max} \approx Z_i^{\max} |U_c|$, where Z_i^{\max} is the maximum ion charge state and $|U_c|$ is given in section 4.2. This means that, with most absorption occurring pre-focus, calculated values for E_{ion}^{\max} are just a few MeV. In fact E_{ion}^{\max} could only approach the 13 MeV detection threshold without the prefocus absorption. Consequently, the null ion data corroborate the previous conclusions about the spatial extent of the energy deposition. Alternatively, had

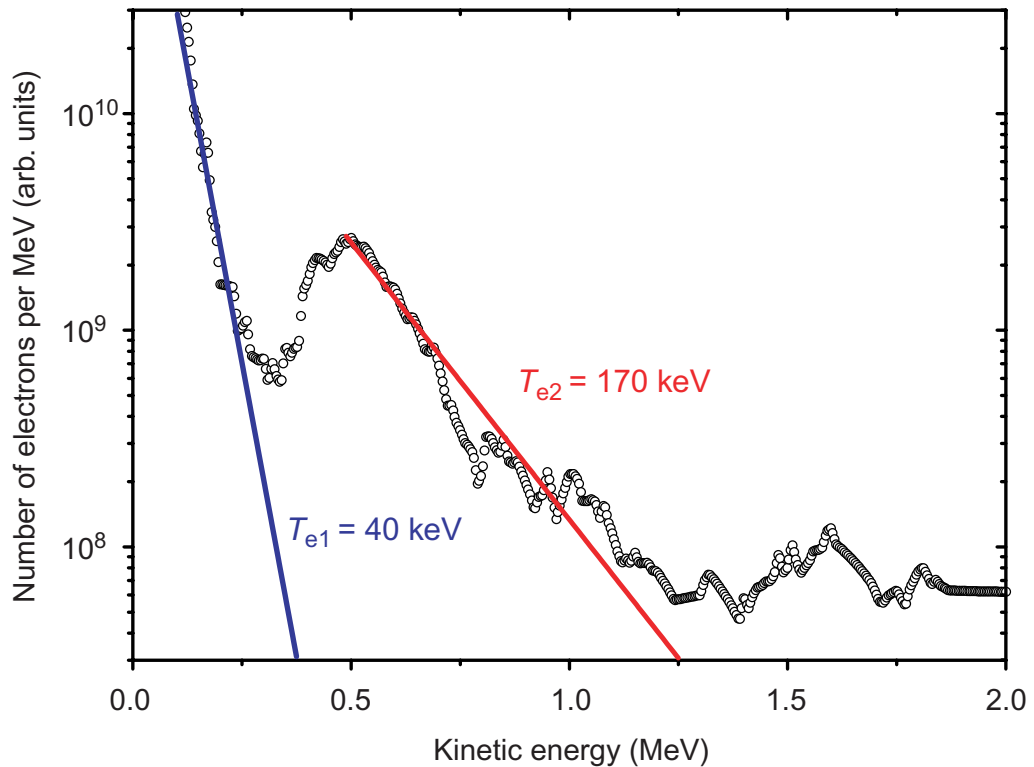


Figure 4. Electron energy spectrum from large Xe gas clusters subjected to relativistic vacuum irradiance, measured using an on-axis magnetic spectrometer and image-plate detector corrected for nonlinear response below 1 MeV. The two Maxwellian fits to the data, given by T_{e1} (blue line) and T_{e2} (red line), compare well to the temperature values calculated for incoherent and coherent collisional heating respectively (section 4.5).

efficient hydrodynamic acceleration occurred, the null ion data imply that the mean electron energies must be below a threshold value of approximately $13 \text{ MeV}/(\Gamma - 1)Z_{\text{eff}}$, which we calculate to be consistent with the estimate in section 4.5 for a maximum T_e value of a few hundred keV. Nonetheless, the irradiances and cluster size used will in practice result in a complicated mix of hydrodynamic and Coulombic expansion following a partial but significant breakdown of whole cluster neutrality, a fact that denotes the ion data as being broadly consistent with our previous findings regarding both the pre-focus absorption and electron temperatures.

4.7. Plasma energy transport analysis and modelling

To further address the observed energy transport, radiation-hydrodynamics simulations were run with laser energy dumps in the NYM code [21], run both LTE and non-LTE and with multi-group radiation transport. Frequency-resolved opacities were taken from IMP [22] and an AWE code (based on an XSN-type non-LTE opacity model [23]), respectively, and SESAME equations of state were used. While showing the highly absorbing Xe medium to be an efficient converter to x-rays—a natural consequence of a high Z target absorbing many Joules of short pulse laser energy without strong electron beam generation—the simulations confirm

insufficient opacity to slow the bulk radiation transport to the v_r , or to stop it in the field-of-view of our imaging system. Therefore, we conclude that the ionization front is not radiation-driven, but is due to electrons. This front originates from laser energy deposition that is decoupled from any bulk material (as opposed to single cluster) transport.

The gross axially asymmetric structures in the ionization seen around $z = 0$ in figures 3(a)–(c) are caused by pre-focus deposition and/or energy moving more freely along $z < 0$ (into lower density regions of the jet) as higher T_e plasma left by the pulse provides increased conductivities. Consideration of the initial temperature scale lengths (after clusters expand and merge) shows that the ionization front possesses a strongly non-local character. Indeed, the n_e profiles in figures 3(a)–(c) are inconsistent with diffusive electron transport, which is characterized by a steep heat front, and instead a bulk, delocalized heat front flows for about tens of ps. While similar in shape to the non-local front observed in cluster experiments conducted at lower irradiances [11], the front we observe is an order of magnitude greater in radial extent, which is roughly consistent with two orders in deposited energy. For these reasons we discount the use of a diffusion-based simulation to solve the inverse problem whereby the absorption coefficient α is iterated until $r_{\text{IF}}(t)$ is re-produced; indeed, simulating nonlocal transport would not necessarily be sufficient without proper consideration of electric field inhibition.

Nevertheless, further useful physical information can be extracted from the probing data. Firstly, by taking the gradient of the trajectory $r_{\text{IF}}(t)$ around time $t = t_0$ in figure 3(d), we can infer that the maximum front speed $v_r^{\text{max}} = dr_{\text{IF}}(t \approx t_0, z = 0)/dt = (9 \pm 4) \times 10^9 \text{ cm s}^{-1}$. The upper bound on v_r^{max} is then consistent with free-streaming electrons at $T_e \approx 32 \text{ keV}$, a value that also lies within the errors of the measured value T_{e1} . Such values for v_r^{max} make clear that the directly absorbed laser energy is distributed among more particles and with significantly lower mean energies than bulk solid target interactions at comparable vacuum irradiances. Secondly, figure 3(b) shows that by $t = t_0 + 15 \text{ ps}$ the ionization front has propagated radially some hundreds of microns out from the z -axis and the volume of ionized material has increased approximately 50-fold over the direct laser heating phase. Simply by assuming that the heating is uniform, we can estimate that the measured T_e should fall by a comparable factor. Thus, dividing by 50 the temperature associated with free-streaming at v_r^{max} gives $T_e \approx 300 \text{ eV}$. For comparison, this temperature value is between that corresponding to free-streaming at \bar{v}_r ($T_e \approx 420 \text{ eV}$), and that for $v_r = dr_{\text{IF}}/dt = 9 \times 10^8 \text{ cm s}^{-1}$ at $t = t_0 + 15 \text{ ps}$ ($T_e \approx 250 \text{ eV}$). Thirdly, by $t = t_0 + 35 \text{ ps}$ (figure 3(c)) the volume of ionized Xe has increased at the expense of the bulk, volumetric thermal energy, the gradients $\partial n_e / \partial r$ have not yet relaxed significantly, and $v_r = 7 \times 10^8 \text{ cm s}^{-1}$. Further out along the jet $v_{z < 0} \approx 4 \times 10^9 \text{ cm s}^{-1}$ (corresponding to free-streaming electrons at $T_e \approx 3 \text{ keV}$), and because $v_{z < 0} > v_r$ it is then nontrivial to deconvolve axial from radial transport effects.

4.8. Laser pre-pulse effects and self-emission data

The highest laser energy ($E_{\text{laser}} = 450 \text{ J}$, $I_0 = 5 \times 10^{19} \text{ W cm}^{-2}$) data are addressed in less detail owing to the high degree of electron stripping and the potential effects of pre-pulse. Whereas the 45 J case gave a single, clean interaction, a 450 J heating pulse produced strongly filamented plasma at t_0 , indicating significant beam break-up. Optical probing showed plasma formation at $t_0 - 700 \text{ ps}$, consistent with contrast levels $I_{\text{pre}}/I_0 \approx 10^{-6}$. Self-focusing may also play a role in beam break-up. That the 450 J shots resulted in very high f_{abs} suggests an even larger absorption

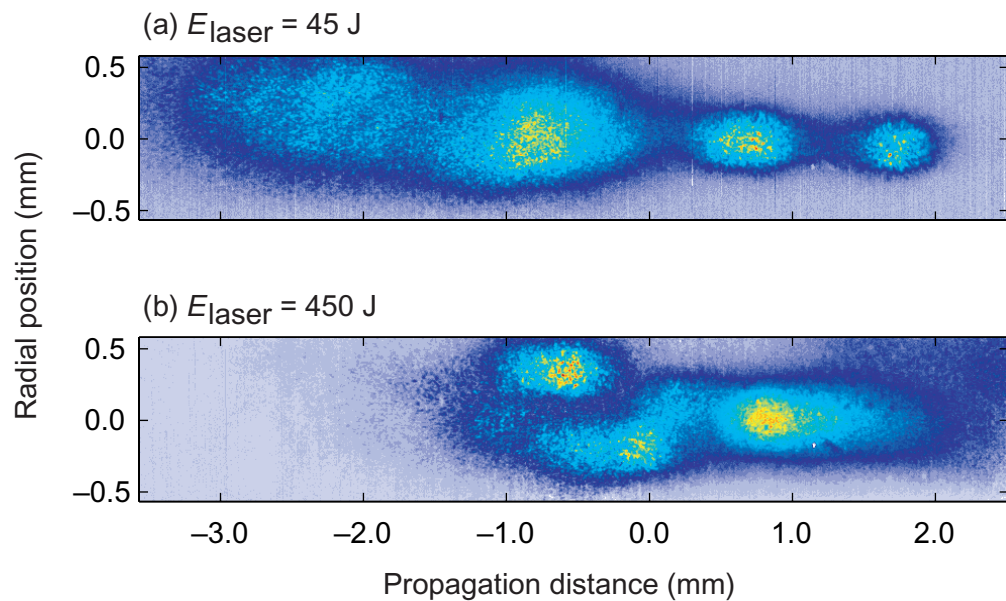


Figure 5. Optical self-emission images from Xe clusters. The high-energy laser pulse travels from left to right. Images are recorded onto a 16-bit CCD camera via dichroic beam-splitters and through a narrow-band interference filter centred at the 1054 nm wavelength of the heating laser. Peak image brightness was equalized using differential neutral density filtering in order to enable relative comparison of the spatial distribution of scattered light at the two laser energies, thereby demonstrating basic differences in the laser–cluster interactions through the gas jet for the two pulse energies, most significantly around the vacuum focus position (propagation distance $z = 0$).

volume than for 45 J shots, as well as greater post-focus fractional deposition owing to cluster disassociation around $z = 0$. This was confirmed by the probing data, which also illustrated the absence of well-defined ionization fronts (owing to the filamentation).

Figure 5 shows side-scatter images recorded along the probe beam line. Long wave pass filtering ($\lambda > 900$ nm) re-produced the 1054 nm filtered images, showing that the emission was not thermal but scattered laser light. Our data are therefore ps time-resolved imaging of the self-emission. In combination, optical probing and self-emission show complex spatial dependencies on the interactions. The two images in figure 5, which are typical for each of the two laser energy bins used, confirm further differences in the interaction physics for the two different laser irradiances; within each energy bin there is good shot-to-shot image repeatability, meaning both the qualitative and quantitative variations are small, particularly compared with the much larger differences observed between these bins. In figure 5(a) the main signal occurs pre-focus and is the result of Rayleigh scattering (consistent with the polarization of the heating laser relative to the image plane). These data are consistent with the finding that most energy is absorbed pre-focus. Post-focus, there is a three-lobe structure between which energy is transported over lengths of the order of 1 mm ($22l_{\text{Rayleigh}}$).

As the critical power for cluster-induced self-focusing is easily surpassed, a stable plasma channel consequently forms, which was observed from shadowgraphy at $t \approx t_0$, and falls

between the first and second lobes. Figure 5(b) also suggests that clusters are destroyed by pre-pulse around the z -axis before the focus. Pre-focus scatter is seen only in the lower irradiance wings of the pulse, implying that the pulse scatters off intact clusters. Also, the more substantial post-focus signal than in figure 5(a) indicates that a greater fraction of laser energy passes through the focus.

5. Conclusions and future directions

A broad set of laser–plasma physics measurements have been conducted using atomic cluster targets and a wide range of laser irradiances extending into the relativistic regime. Each experiment revealed new findings, which have been analysed throughout using appropriate modelling.

In the first instance, a table-top TW class, sub-ps laser provided a range of high but sub-relativistic irradiances to heat Kr clusters, and continuum x-ray spectroscopy was employed for direct measurements of the plasma electron temperatures. In these data, new and compelling evidence of multi-keV resonant cluster heating is seen as the irradiance is varied. Very high material energy densities are created, although diminishing heating efficiency towards a peak vacuum irradiance of $I_0 \approx 10^{17} \text{ W cm}^{-2}$ is observed. Modelling of these data has shown agreement, for the first time, with both collisional and collisionless heating mechanisms specific to clusters—the latter included combining and extending existing models [2, 10]. While furthering our understanding of sub-relativistic laser–cluster interactions, these data and the accompanying analysis also underscore their inherent complexity and the need for a single comprehensive model of the laser–plasma physics at these irradiances.

Complementary experiments, conducted with a large facility laser of the same FWHM pulse duration and central wavelength as the table-top system, provide the first measurements of energy deposition in a high Z (Xe) atomic cluster medium using both high energies and relativistic vacuum irradiances. Despite modelling indicating an upper irradiance limit $I \approx 10^{18} \text{ W cm}^{-2}$ for efficient single cluster absorption, the measured absorption fractions were close to unity at vacuum irradiances (I_0) much higher than this limit. A small reduction in the absorption fraction for the highest irradiance ($I_0 = 5 \times 10^{19} \text{ W cm}^{-2}$) was well correlated with the observation of destructive pre-pulse effects in the vicinity of the vacuum focus. These effects were observed both actively, through time- and space-resolved optical probing, and through passive self-emission measurements. Using a laser irradiance of $I_0 = 5 \times 10^{18} \text{ W cm}^{-2}$, these pre-pulse effects were not in evidence. In this case, probing confirmed substantial pre-focus deposition, and allowed measurements of plasma energy transport which demonstrated the absorbed energy per cluster to be greatest around the best focus. As a result of this heating, a fast electron-driven ionization front with speeds of the order of 10^9 – $10^{10} \text{ cm s}^{-1}$ was launched radially outwards.

Electron spectroscopy revealed that the focal region reached electron temperatures of at least tens of keV—from which peak energy densities of $\varepsilon \approx 10^8 \text{ J cm}^{-3}$ are inferred—as well as evidence of heating a separate group of electrons to temperatures of 170 keV. Analysis has shown that both the electron data and null high energy ion measurements are consistent with high pre-focus absorption.

Despite the limitations imposed by a relatively ‘long’ laser pulse length of 500 fs and the eventual onset of pre-pulse effects, our data demonstrate a route to creating super-heated plasma

without the electron beam generation that dominates in macroscopic solid targets. Evidently, superior laser contrast would be essential for generating still greater values of ε , and could be met, for example, through the use of a plasma mirror, burn-through foil, frequency-doubling or other nonlinear mechanisms to suppress the pre-pulse. Higher laser irradiances than utilized in the work described in this article would also require a shorter pulse and/or larger cluster sizes to prove productive. Even then, focusing to a well-defined (supersonic) gas jet boundary may be required to avoid energy losses or beam filamentation before the best focus. Together, these improvements would extend the range of high energy densities accessible with cluster targets for applications such as the laboratory generation of strong, radiative shocks [24] of astrophysical relevance, and should facilitate the use of clusters as an intense, prompt multi-keV x-ray source to use, for example, as a Thomson scattering probe, or for the back-lighting or driving of a secondary laser target with the particular advantage of being able to readily mix gases to tailor the emission spectrum. Focusing both to and across the gas jet boundary would also help counter x-ray source size increases associated with pre- and post-focus absorption.

Acknowledgments

The support of the RAL laser and target area staff is gratefully acknowledged, as are useful discussions with Brian Thomas and Colin Smith. This work was funded by the UK MoD and the EPSRC.

References

- [1] Posthumous J 2001 *Molecules and Clusters in Intense Laser Fields* (Cambridge: Cambridge University Press)
- [2] Taguchi T, Antonsen T M Jr and Milchberg H M 2004 Resonant heating of a cluster plasma by laser light *Phys. Rev. Lett.* **92** 205003
- [3] Gibbon P 2005 *Short Pulse Laser Interactions with Matter: An Introduction* (London: Imperial College Press)
- [4] Madison K W, Patel P K, Allen M, Price D, Fitzpatrick R and Ditmire T 2004 Role of laser-pulse duration in the neutron yield of deuterium cluster targets *Phys. Rev. A* **70** 053201
- [5] Danson C *et al* 2004 Vulcan Petawatt—an ultra-high-intensity interaction facility *Nucl. Fusion* **44** S239
- [6] Hagen O F 1992 *Rev. Sci. Instrum.* **63** 2374
- [7] Isaac R C, Vieux G, Ersfeld B, Brunetti E, Jamison S P, Gallacher J, Clark D and Jaroszynski D A 2004 Ultra hard x-rays from krypton clusters heated by intense laser fields *Phys. Plasmas* **11** 3491
- [8] Ditmire T, Donnelly T, Rubenchik A M, Falcone R W and Perry M D 1996 Interaction of intense laser pulses with atomic clusters *Phys. Rev. A* **53** 3379
- [9] Kim K Y, Alexeev I, Parra E and Milchberg H M 2003 Time-resolved explosion of intense-laser-heated clusters *Phys. Rev. Lett.* **90** 023401
- [10] Briezman B N, Arefiev A V and Fomyts'ki M V 2005 Nonlinear physics of laser-irradiated microclusters *Phys. Plasmas* **12** 056706
- [11] Ditmire T, Gumbrell E T, Smith R A, Djaoui A and Hutchinson M H R 1998 Time-resolved study of nonlocal electron heat transport in high temperature plasmas *Phys. Rev. Lett.* **80** 720
- [12] Krainov V P and Smirnov M B 2002 *Phys. Rep.* **370** 237
- [13] Ditmire T, Smith R A, Tisch J W G and Hutchinson M H R 1997 High intensity laser absorption by gases of atomic clusters *Phys. Rev. Lett.* **78** 3121
- [14] Rose-Petrucci C, Schafer K J, Wilson K R and Barty C P J 1997 Ultrafast electron dynamics and inner-shell ionization in laser driven clusters *Phys. Rev. A* **55** 1182

- [15] Jungreuthmayer C, Geissler M, Zanghellini J and Brabec T 2004 Microscopic analysis of large-cluster explosion in intense laser fields *Phys. Rev. Lett.* **92** 133401
- [16] Seely J F and Harris E G 1973 Heating of a plasma by multiphoton inverse bremsstrahlung *Phys. Rev. A* **7** 1064
- [17] Petrov G M, Davis J, Velikovich A L, Kepple P C, Dasgupta A, Clark R W, Borisov A B, Boyer K and Rhodes C K 2005 Modelling of clusters in a strong 248-nm laser field by a three-dimensional relativistic molecular dynamic model *Phys. Rev. E* **71** 036411
- [18] Deiss C, Rohringer N, Burgdörfer J, Lamour E, Prigent C, Rozet J-P and Vernhet D 2006 Laser-cluster interaction: x-ray production by short laser pulses *Phys. Rev. Lett.* **96** 0132203
- [19] Mulser P, Kanopathipillai M and Hoffmann D H H 2005 Two very efficient nonlinear absorption mechanisms in clusters *Phys. Rev. Lett.* **95** 103401
- [20] Ditmire T, Zweiback J, Yanovsky V P, Cowan T E, Hays G and Wharton K B 1999 Nuclear fusion from explosions of femtosecond laser-heated deuterium clusters *Nature* **398** 489
- [21] Roberts P D, Rose S J, Thompson P C and Wright R J 1980 *J. Phys. D: Appl. Phys.* **13** 1957
- [22] Rose S J 1992 *J. Phys. B: At. Mol. Opt. Phys.* **25** 1667
- [23] Lokke W A and Grasberger W H 1977 XSNQ-U— non-LTE emission and absorption coefficient subroutine *Lawrence Livermore Laboratory Report UCRL-52276*
- [24] Moore A S, Gumbrell E T, Lazarus J, Hohenberger M, Robinson J S, Smith R A, Plant T J A, Symes D R and Dunne M 2008 Full trajectory diagnosis of laser-driven radiative blast waves in search of thermal plasma instabilities *Phys. Rev. Lett.* **100** 055001